analytical chemistry

ARTICLE

pubs.acs.org/ac

Microscale MALDI Imaging of Outer-Layer Lipids in Intact Egg Chambers from *Drosophila melanogaster*

Pawel L. Urban,[†] Chia-Hsien Chang,[†] June-Tai Wu,[‡,⊥,§] and Yu-Chie Chen*[,†]

[†]Department of Applied Chemistry, National Chiao Tung University, Hsinchu, Taiwan

[‡]Institute of Molecular Medicine, College of Medicine, and [§]Research Center for Developmental Biology and Regenerative Medicine, National Taiwan University, Taipei, Taiwan

[⊥]Department of Medical Research, National Taiwan University Hospital, Taipei, Taiwan

Supporting Information

ABSTRACT: Fruit fly (*Drosophila melanogaster*) is a standard model organism used in genetics and molecular biology. Phospholipids are building blocks of cellular membranes, and components of a complex signaling network. Here, we present a facile method, based on matrix-assisted laser desorption/ionization (MALDI) mass spectrometry (MS), for molecular imaging of phospholipid distributions in submillimeter-sized components of the fruit fly reproductive system. Individual egg chambers were deposited on a specially prepared MALDI target comprising an aluminum slide with a rough surface created by ablation with a microsecond-laser: this helped to immobilize biological specimens, remove excess of saline solution by adhesive forces, carry out microscopic observations, and facilitated distribution of the MALDI matrix. A continuous-flow ultrasound-assisted spray was used for the deposition of MALDI matrix (9-aminoacridine) onto the sample. The upper surface of the specimen was then scanned with a 355-nm solid-state laser with a preset beam focus of 10 μm to obtain negative-ion mode MALDI-MS images. Overall, this provided sufficient spatial resolution to reveal micrometer-scale gradient-like patterns of phospholipids along the anterior/posterior axis of egg chambers. Several phosphatidylinositols are seen to be segregated according to the number of unsaturated bonds, with an elevated abundance of polyunsaturated phosphatidylinositols within the oocyte compartment.

Matrix-assisted laser desorption/ionization (MALDI) mass spectrometry (MS) has already been shown to be applicable to analysis of metabolites in cells (e.g., refs[1−4]). MALDI-MS can readily be implemented in molecular imaging[5] (for reviews, see for example refs [6−12]), a technique that is transforming the way in which biological tissues can be analyzed. Using tightly focused laser beams and fast scan rates, it is now possible to obtain high-resolution molecular images and perform histological analyses based on the partitioning of biomolecules between the layers of metabolically dissimilar cells.[13] Obtaining high quality molecular images of tissues also requires appropriate sample preparation.[7,12]

Fruit fly (*Drosophila melanogaster*) is a common model organism used in molecular and developmental biology.[14,15] During oogenesis, the developing oocytes are accompanied by nurse and follicle cells within a microscopic unit, called "egg chamber" (Figure S1, Supporting Information). Nurse cells provide nutrients and developmental control molecules to the oocyte. Follicle cells, initially surrounding the egg chamber, group around the oocyte cell in the course of oogenesis. The so-called "border cells" migrate from the anterior pole toward the border between the nurse cells and the oocyte.[16] Some of the genes that control organization of cells during oogenesis and embryonic development relate to the synthesis of phospholipids, which are present in cell membranes.[17] In fact, among various classes of biomolecules, phospholipids are important building elements of all cellular membranes, and major components of a complex intracellular signaling network.[18] Polyunsaturated lipids influence protein−lipid interaction, as well as order, dynamics, and transport properties of biological membranes.[19] According to the "membrane pacemaker" theory of metabolism, the relative balance between monounsaturated and long-chain polyunsaturated acyl chains in membrane bilayers is a fundamental determinant of metabolic rate of a species.[20] Therefore, one motivation for this study was to develop a mass spectrometric method, based on high-resolution MALDI imaging, which would enable molecular characterization and mapping of phospholipids present in the outer (membrane-rich) layers of egg chambers in fruit fly.

MALDI-MS,[13,21−23] as well as a related technique, matrix-free laser desorption/ionization (LDI) mass spectrometry,[24,25] are convenient platforms for studying distributions of small-molecule

Received: February 24, 2011
Accepted: April 8, 2011
Published: April 26, 2011

metabolites, such as phospholipids, in biological tissues. As demonstrated in earlier work, MALDI-MS can readily be used to study localization of neuropeptides in single neurons.[26] Subcellular resolution could also be attained for several intracellular molecules using the LDI-MS technique.[27] Secondary-ion mass spectrometry (SIMS) provides submicrometer spatial resolution;[28−30] however, because of the extensive fragmentation observed in SIMS, its applicability to micrometabolomic studies has so far been limited. State-of-the-art MALDI-MS instrumentation can provide a spatial resolution that is sufficient for numerous imaging applications.[13] Despite demonstration of several protocols for MALDI-MS analysis on the cellular and subcellular level (for a review on single-cell MS, see, for example, ref 31), preparation of microscopic samples (such as cells or small cell ensembles) for MALDI imaging is still challenging. Issues to address encompass artifact-free sample handling, preservation of the native chemical composition, and targeting analyte molecules in specific cell compartments. For example, by carefully optimizing the sample preparation step, peptide concentrations in distinct cell types present within ganglions of *Aplysia californica* could be determined without isolating individual cells.[32] Specialized sample preparation protocols (such as the "stretched sample method", based on fragmenting samples into thousands of spatially isolated islands[33]) as well as thorough optimization of the methodological and instrumental toolkit[12] can improve resolution of MALDI imaging procedures to enable observations at the cellular level.

It is apparent that most sample preparation methods for MALDI imaging involve slicing organs and tissues; therefore, they allow one to probe intracellular metabolites and proteins with the MALDI laser beam (e.g., refs 6−11, 34−37). MALDI imaging executed in this format has become an enabling tool for research in biomedicine. Nevertheless, cutting tissues into thin sections leads to significant disruption of biological membranes. In order to study chemistry of the outer surface of cells as well as cellular interfaces, a sample preparation method that avoids slicing would be helpful. Here we demonstrate a facile protocol for microscale sample preparation, which allows one to obtain MS images revealing biochemical phenomena occurring in the outer layer of egg chambers in the fruit fly. In summary, submillimeter-sized components of the reproductive system are placed on a rough surface of an aluminum slide, which has been modified by ablation with a microsecond-laser. Excess saline buffer is removed instantly by capillary forces, and the sample firmly adheres to the rough surface. Following microscopic observation of the cell ensemble, and application of a lipophilic cocktail of the MALDI matrix (aided by a continuous-operation ultrasound-assisted spray), a high-resolution MALDI-MS scan is carried out. The MS images, obtained this way, reveal site-specific localization of various lipid components within individual egg chambers.

EXPERIMENTAL SECTION

Fabrication of Sample Supports for MALDI Imaging. Sample supports, such as indium tin oxide (ITO)−glass, ITO−glass coated with polysilazane, channel arrays ablated on a glass surface, aluminum, aluminum coated with silica (including disposable thin-layer chromatography plates (Merck, Darmstadt, Germany)), titanium, and titanium ablated with a laser, have all been tested with limited success. Eventually, we opted for aluminum slides ablated with a microsecond-laser because they exhibited the most favorable characteristics.

The microsecond-laser engraving machine, SDPL-50W (Sintec Optronics Pte, Singapore), is equipped with a Nd:YAG DPSS laser (λ = 1064 nm) and controlled by Laser Marker software (version 3.2.3.5; JiNan DuoWei Laser Technology, Jinan, Shandong, China). In order to create a MALDI target for microscale imaging, the laser beam was rastered in X and Y directions over a rectangular area (typically, 2 × 2 mm) on the surface of the aluminum slide. The following parameters were used: laser frequency, 2000 Hz; pulse width, 8 μs; hatch gap, 10 μm (double lines). Further on, the ablated slides were cleaned with ethanol and water to remove the deposit of aluminum oxide next to the ablated sites, and sonicated in a mixture of ethanol and water (∼1:1, v/v). Dry slides were directly used for deposition of specimens.

Fly Stocks and Cell Culture. Fruit flies (*Drosophila melanogaster*; w^{1118}; *p{ubi-nls-GFP}*, expressing green fluorescent protein (GFP)) were reared at room temperature on a standard organic medium (composed of yeast, soy flour, yellow cornmeal, light malt extract, light corn syrup, propionic acid, and agar) loaded into plastic vials. The culture of *Closterium acerosum* was maintained in Alga-Gro freshwater medium (Carolina Biological Supply Company, Burlington, NC). Cells were resuspended in pure water prior to further preparation for the MALDI imaging experiment (identical with the preparation of the egg chamber samples). The photoperiod for the fly stocks and culture of algal cells was set to 16-h day/8-h night. Illumination was provided by fluorescent lamp.

Dissection of Fruit Flies. Before each experiment, flies were anesthetized with CO_2. Female individuals were manually dissected under a stereodissecting microscope (Nikon, Tokyo, Japan) with a set of precise tweezers (cat. no. 0203-5-PO; Dumoxel; Dumont, Montignez, Switzerland) and fine scissors (cat. no. 15005-08; FST, Heidelberg, Germany). The dissected organs were stored in phosphate-buffered saline (PBS) solution (see Supporting Information) for the maximum time period of 8 h, in case further handling was delayed. Ovaries were separated into ovarioles and egg chambers of different developmental stages according to a standard protocol.[38] Digestion with collagenase ($\leq$10 mg mL^{-1} in PBS, $\geq$ 10 min, room temperature) was initially attempted to facilitate separation of individual egg chambers from ovarioles; however, this step weakened the structure of egg chambers, which then became more prone to damage. To verify the differences in the phospholipid composition of the nurse-cell and oocyte sections, the egg chambers were cut using a stainless-steel blade (Micra, Solingen, Germany) and separated into two parts.

Preparation of Microscopic Samples. Single cells of *Closterium acerosum* or individual egg chambers from *Drosophila melanogaster* were easily deposited on the ablated surface of aluminum slides using a micropipet with a tip having an extra-large opening (>0.5 mm). A short strip of filter paper (e.g., ∼5 × 20 mm) was used to remove the excess of PBS buffer surrounding the specimen. When a corner of the paper strip was touched to the droplet inside the recipient site ablated with the microsecond-laser, the solution was immediately removed because of the action of capillary forces. Devoid of suspension medium, the specimen firmly adhered to the rough laser-ablated surface. This is opposed to slow evaporation of the suspension medium, in which case leakage of yolk from the oocyte likely occurs. The egg

chambers, stretched on the ablated area of aluminum slide, were initially imaged using an upright fluorescence microscope (Eclipse 80i; Nikon) equipped with a superhigh-pressure mercury lamp (100 W) and a digital camera (DS-Ri1). The following filters were used: UV-2A (excitation 330−380 nm) and B-2A (450−490 nm). Optical and fluorescence imaging was followed by application of a MALDI matrix.

Following a series of preliminary experiments, in the final version of the protocol, we used a continuous-operation ultrasonic spray: The MALDI matrix solution was delivered with a syringe pump (cat. no. 780100; kdScientific, Holliston, MA) at a rate 3−6 mL h^{-1}, via polytetrafluoroethylene tube onto the nozzle of an ultrasonic transducer (Dental Ultrasonic Scaler, DTE D1; Woodpecker Medical Instrument Company, Guilin, Guangxi, China), operated continuously at ∼28 kHz and ∼5 W. After having tested various solvent mixtures and concentrations (3−9 mg mL^{-1}), we decided to use a 3 mg mL^{-1} solution of 9-aminoacridine dissolved in hexane/acetone (1:2, v/v), as MALDI matrix. Typically, an amount of 1−2 mL of the matrix cocktail was spent per target containing six sample recipient sites. Thus, the spraying time was normally 20−40 min. Application of the matrix onto the target was carried out under a fume cupboard, and personal safety items, such as gloves, safety glasses, dust mask, and lab coat, were in use. For MALDI imaging, the aluminum slides were attached to the conductive surface of ITO−glass with double-sided adhesive copper tape and mounted on a metal carrier.

MALDI-MS. For MALDI imaging experiments, we used an Autoflex III Smartbeam MALDI-time-of-flight (TOF)-MS instrument from Bruker Daltonics (Bremen, Germany), equipped with a solid-state laser (λ = 355 nm). Using the 9-aminoacridine matrix, the instrument was operated in the negative-ion mode with the following settings: ion source 1, −19.0 kV; ion source 2, −16.7 kV; lens, −9 kV; delay time, 0 ns. In all the imaging experiments, the laser beam focus was set to 10 μm, and the default spacing of the scan raster was 15 μm; 15−20 laser shots were fired at each raster point with the preset frequency of 50 Hz. Laser intensity was adjusted in a series of preliminary experiments to obtain high signal-to-noise ratio with a limited number of shots. The mass range was normally set to 400−1500 Da, and all the ions up to 400 Da were deflected to avoid saturation of the microchannel plate detector. Data were acquired using the flexControl software (version 3.0; Bruker Daltonics) while the imaging experiments were facilitated by the flexImaging software (version 2.0; Bruker Daltonics). Metabolite and peptide standards were routinely added to one of the recipient sites on each slide, so as to enable calibration prior to imaging.

In order to identify unknown metabolites, we carried out MS/MS analysis using a laser-induced fragmentation technology (LIFT) system built in the Autoflex instrument. In order to measure accurate mass of unknown peaks in MS, we also performed high-resolution and high mass accuracy measurements on the Fourier transform ion cyclotron resonance (FTICR)-MS instrument (Apex-Qe SHEDS, 9.4 T; Bruker Daltonics) equipped with an electrospray and a MALDI ion source. The FTICR mass spectrometer was initially calibrated using sodium formate clusters under electrospray conditions. Several internal standards with masses lower and higher than the masses of the analyte molecules were mixed with the sample for subsequent internal calibration. Accurate mass measurements were followed by database search (HMDB (www.hmdb.ca), METLIN (metlin.scripps.edu)).

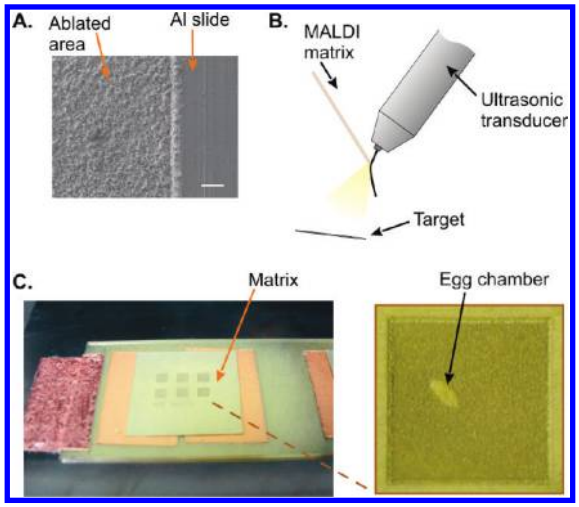

Figure 1. Microscale sample preparation for MALDI imaging. (A) Scanning electron micrograph of the aluminum slide with rough surface created by ablation with a microsecond-laser. (B) Applying a MALDI matrix cocktail to the microscopic biological samples by means of ultrasound-assisted spray. (C) An array of ablated recipient sites after application of the MALDI matrix. The inset shows a sample (egg chamber) immobilized on the rough area of the aluminum slide and coated with yellow crystals of the 9-aminoacridine matrix. Scale bar in A: 100 μm. Size of the individual recipient site in C: 2 × 2 mm.

RESULTS AND DISCUSSION

In order to support a study of metabolic processes associated with oogenesis, we aimed to map phospholipid distributions in the outer (membrane-rich) layer of egg chambers obtained from dissected fruit flies (*Drosophila melanogaster*). Since MALDI-MS offers the possibility to execute multiple sample preparation steps using multifunctional MALDI target plates (for a review, see ref 39), the protocol proposed here integrates microscale sample immobilization, removal of the suspension liquid, optical and fluorescence microscopy, ultrasound-assisted matrix deposition, and high-resolution MALDI imaging.

Laser-Ablated Sample Support and Application of Matrix by Ultrasound-Assisted Spray. Laser technology has already proven useful in fabrication of analyte-enrichment MALDI supports,[40,41] matrix-free LDI supports,[42] and high-density microarrays for mass spectrometry.[43] Here, a microsecond-laser beam was used to fabricate sample supports which contain 2 × 2-mm-sized ∼40-μm-deep recipient sites with a rough surface (Figure 1A). The experience gathered in this study suggests that this surface can assist preparation of microscale biological specimens, such as egg chambers, for MALDI imaging through instantaneous immobilization combined with depletion of PBS solution (see Experimental Section) as well as absorption of excessive amounts of the matrix cocktail delivered by ultrasound-assisted spray.

9-Aminoacridine was introduced as a MALDI matrix by Vermillion-Salsbury and Hercules[44] and has successfully been used for analysis of primary metabolites in cells.[1−4,36,43,45] Here, the 9-aminoacridine matrix is utilized for detection of phospholipids in negative-ion mode at moderate laser power. Under these conditions, phospholipids are predominantly detected as anions formed by deprotonation, as opposed to adduct ions, which makes interpretation of the resulting mass spectra straightforward. To facilitate mixing and cocrystallization of the nonpolar

matrix with the target analytes (lipids), 9-aminoacridine was dissolved in a mixture of hexane and acetone. Because of the lipophilic nature of this solution, the microdroplets (sprayed above the sample) attach to the hydrophobic surface of egg chamber. The resulting matrix crystals cover the outer surface of the specimen; however, they are not seen within the central region of the section of a late-stage egg chamber sample, visualized by microscopy (Figure S2, Supporting Information). Importantly, droplets of the matrix cocktail prepared with hexane and acetone evaporate immediately after landing on the target. This is opposed to using less volatile solvents, such as acetonitrile or ethanol, in which case the droplets merge and wet the whole area of the recipient site (not shown). Excess of liquid, that cannot be absorbed within the rough area of aluminum target, may contribute to translocation and dispersion of analytes from the specimen.

Since application of intense ultrasound to a liquid−gas interface leads to generation of both mist and vapor from the liquid,[46] here we utilized a continuous-operation ultrasonic sprayer to deposit 9-aminoacridine matrix onto microscopic samples (Figure 1B). This provided satisfactory coverage of the specimen, as well as the adjacent area, with a thin layer of matrix crystals (Figure 1C). Despite its inherent simplicity and low consumption of the toxic matrix cocktail, an important advantage of using the ultrasonic sprayer is that the microscopic specimens are not exposed to the nebulizer gas flow (characteristic of gas-powered sprayers), which reduces the risk of the specimen being moved from its original position on the recipient site.

High Spatial-Resolution MALDI Imaging of Microscale Specimens. Various methods can be used to evaluate spatial resolution of MS imaging protocols (e.g., using electron microscopy grids,[47] or fingerprints[48]). In the present work, to ascertain that the spatial resolution of the sample preparation method is sufficient for visualizing phospholipid distributions on a micrometer scale, we used microscopic unicellular algae (*Closterium acerosum*; Figure 2A) as test samples. As exemplified in Figure 2B, the distributions of some molecules, which appear in *C. acerosum* and give rise to prominent MALDI-MS signals, are essentially contained within the footprints of the rod-shaped cells observed by microscopy. This leads to a conjecture that the components of the cell, which are mapped by the method presented here (comprising sample deposition on aluminum slides ablated with a microsecond-laser, followed by matrix application using ultrasonic spray), correspond to the real ones, within a precision limit of tens, rather than hundreds, of micrometers (see also Figure S3, Supporting Information). Considering the width of the *C. acerosum* cell (30−50 μm), and the mean spacing of the laser raster in the MALDI scan (15 μm), one should anticipate that two to three discrete sampling positions across the smaller dimension of the cell are scanned with the laser beam: this estimate is reflected in the overlay of the raster used and the MALDI image regions (negative-ion m/z 745.5 and 831.5, Figure 2B). In the case of the cell depicted in Figure 2, some ions (m/z 831.5, and 829.5 (not shown)) were almost equally distributed within the whole-cell contour, while the others (m/z 745.5, and 743.5 (not shown)) were predominantly detected in one of the two semicells: for example, the signal at the m/z 745.5 was higher in the semicell that appears brighter in the optical micrograph (Figure 2A). This suggests the possibility of performing chemical mapping of individual cells by MALDI-MS.

The advantage of using *C. acerosum* to evaluate the quality of the MALDI imaging procedure is that these rod-shaped cells have a relatively high aspect ratio, and the lateral resolution can directly be tested on a biological sample. In other study, smaller algal cells could also be analyzed by matrix-free LDI-MS.[49] However, the high laser fluence used in that study caused significant disruption of the cells, which degraded original distribution of metabolites. The microscale sample preparation presented here allows one to record MS signals of multiple metabolites at relatively low laser power while preserving integrity of individual cells. Even the features of biological specimens that are smaller than 50 μm could readily be visualized in the MALDI images. Therefore, in the next step, we attempted to use this method for imaging early developmental-stage fruit fly egg chambers (Figure 3A). Phospholipid peaks with high signal-to-noise ratios were recorded for every 10-μm-sized pixel within the sample area using 20 laser shots only. Also in this case, the contours of individual egg chambers were very sharp, and the target analytes with molecular weight greater than 650 Da did not disperse beyond the boundaries of the specimens (Figure 3B). While low-molecular-weight metabolites (M_w < 650 Da) exhibit a greater mobility and do disperse beyond the contours of the specimens (in particular, when higher flow rates of the matrix cocktail are used; not shown), further results refer to the lipid components of biological membranes (M_w > 650 Da), which are not notably translocated because of the contact with the MALDI matrix cocktail.

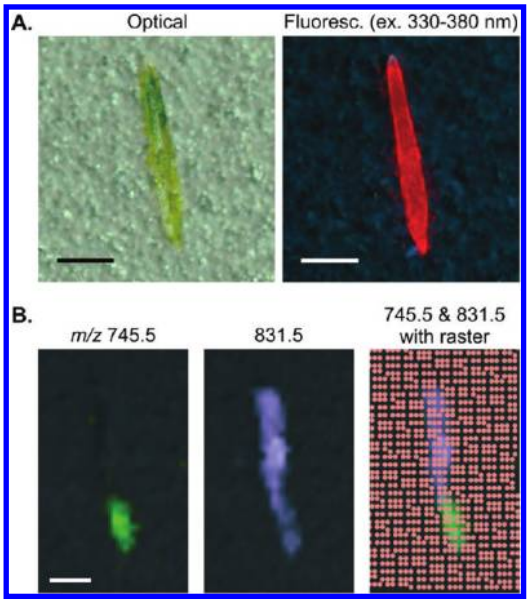

Figure 2. Application of the proposed method to single-cell imaging. (A) Optical and fluorescence micrographs of a selected algal cell (*Closterium acerosum*) deposited on the aluminum slide ablated with a microsecond-laser. (B) MALDI images displaying signal strengths of two chosen ions (putatively assigned as phospholipids) that have been detected during the negative-ion mode MS scan. The last image in B represents an overlay of the raster used, with pink dots corresponding to the laser scanning positions, and the MALDI image regions. Scale bars: 100 μm.

Unknown Peaks in MALDI Spectra of Fruit Fly Egg Chambers. Identification of the small-molecule analytes present in egg chambers of fruit flies, which give rise to the MALDI-MS signals, such as those in Figure 3C, was carried out in the following way: First, we assumed the compounds of interest belong to lipids based on the characteristic peak intensity distribution with a 2-Da

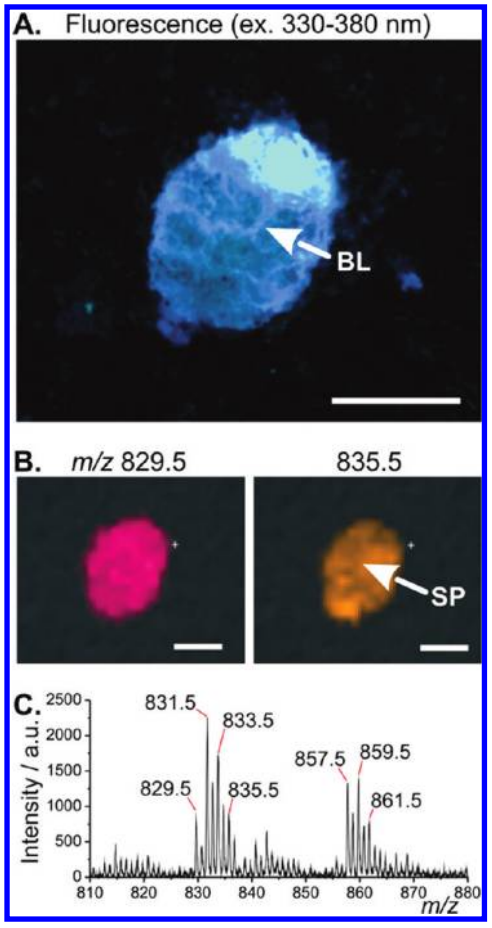

Figure 3. MALDI imaging of an egg chamber at its early developmental stage (*Drosophila melanogaster*, strain w^{1118}, *p*{*ubi-nls-GFP*}). (A) Fluorescence image of the sample prepared on the aluminum slide ablated with a microsecond-laser, prior to the application of MALDI matrix. (B) MALDI images obtained according to the protocol presented. The bright region in A corresponds to the oocyte cell located near the posterior pole. One of the border lines separating cells in A has been marked with an arrow (BL). Scale bars in A and B: 100 μm. (C) A MALDI spectrum corresponding to the central region of the specimen (indicated by an arrow in B, SP).

mass difference within a given group of peaks. Second, we measured the accurate masses using MALDI-TOF-MS (Table S1, Supporting Information) and MALDI-Fourier transform ion cyclotron resonance (FTICR)-MS (Table S2, Supporting Information). Matching the measured accurate masses with the exact masses of various phospholipids listed in metabolite databases, such as HMDB (www.hmdb.ca) or METLIN (metlin.scripps.edu), gave us hints on the possible identities of the species detected. Third, we carried out MS/MS analysis using the laser-induced fragmentation technology (LIFT) system and compared the fragment spectra obtained for the real samples with that obtained during analysis of a standard compound. For MS peaks belonging to the two groups in the m/z ranges 829.5−835.5 and 857.5−863.5, we noted a very good agreement of fragment spectra with that of phosphatidylinositol, containing the characteristic fragment peaks: PO_3^-, m/z = 79, $H_2PO_4^-$, m/z = 97, $C_3H_6O_5P^-$, m/z = 153, and most importantly, $C_6H_{10}O_8P^-$, m/z = 241; Figure S4, Supporting Information.

Gradient-like Distribution of Phospholipids in Late-Stage Egg Chambers. Further on, we conducted a series of MALDI imaging experiments on egg chambers in late developmental stages, which had been isolated from two strains of fruit flies (w^{1118}; *p*{*ubi-nls-GFP*}, and w^{1118}). Contrary to the result obtained for an early stage egg chamber (Figure 3), the MALDI images collected for egg chambers in later stages revealed a gradient-like distribution of various phospholipid species along the anterior/posterior axis (Figure 4). Because of the high protein content in yolk (blue fluorescence with the excitation wavelength 330−380 nm), and relatively high level of GFP expression within the nurse cells (in the w^{1118}; *p*{*ubi-nls-GFP*}, green fluorescence with the excitation wavelength 450−490 nm), it was easy to map internal architecture of an egg chamber, stretched on the laser-ablated aluminum slide, by means of fluorescence microscopy (Figure 4A). The image results obtained for both strains show that two kinds of phosphatidylinositols, in the m/z ranges 829.5−835.5 and 857.5−863.5 (differing by two CH_2 groups in the fatty acid chain; cf., Figure 4B), are segregated in the egg chambers according to the number of unsaturated bonds present in the fatty acid chains. This segregation is especially clear in the egg chambers, in which the oocyte occupies half of the egg chamber volume (cf., Figure S5, Supporting Information). Approximately, from stage 9 until stage 11 of the egg chamber development, phosphatidylinositols with one unsaturated bond preferentially localized in the outer layer of the part occupied by the nurse cells, while phosphatidylinositols with four unsaturated bonds localized in the part occupied by the oocyte (Figure 4C−E). In earlier stages, there was no clear borderline between the areas occupied by the above-mentioned forms (Figure 4C). However, this borderline was clear and sharp in the egg chambers in stage 10 (Figure 4A and 4D), as observed in the results obtained for both strains (see also Figure S5). The ability to record such gradients in samples of up to a few hundred micrometers, which consist of just a few cells, and with high reproducibility (>10 samples investigated) points to high analytical capabilities of the protocol used.

Moreover, one could also observe transient distributions of phosphatidylinositols with two and three unsaturated bonds; these also localized preferentially in the nurse-cell and oocyte-occupied compartments, respectively (Figure 4A: m/z 833.5 vs 831.5, and 861.5 vs 859.5). However, a lower intensity of these two components was also observed in the counterpart sections of the egg chambers. Apart from the two features in the m/z ranges 829.5−835.5 and 857.5−863.5, several other MS signals revealed gradient-like distribution in the egg chambers (not shown). The observed MS image patterns clearly match the compartmentalization of the egg chambers into oocyte and nurse cells visualized by optical and fluorescence microscopy (Figure 4A). This emphasizes the usefulness of combining multiple detection systems with mass spectrometry when studying small ensembles of cells. Note that the expression of GFP did not seem to affect the distribution of phosphatidylinositols in egg chambers.

Localization of Phospholipids According to the Number of Double Bonds. In order to prove that the apparent gradient-like distributions of phospholipids (Figure 4) reflect the real condition, we have carried out a control experiment in which the oocyte part was physically detached from the nurse-cell-occupied part (Figure 5A). In this experiment, the two parts were deposited separately onto two different recipient sites of the aluminum slide ablated with a microsecond-laser (Figure 5B).

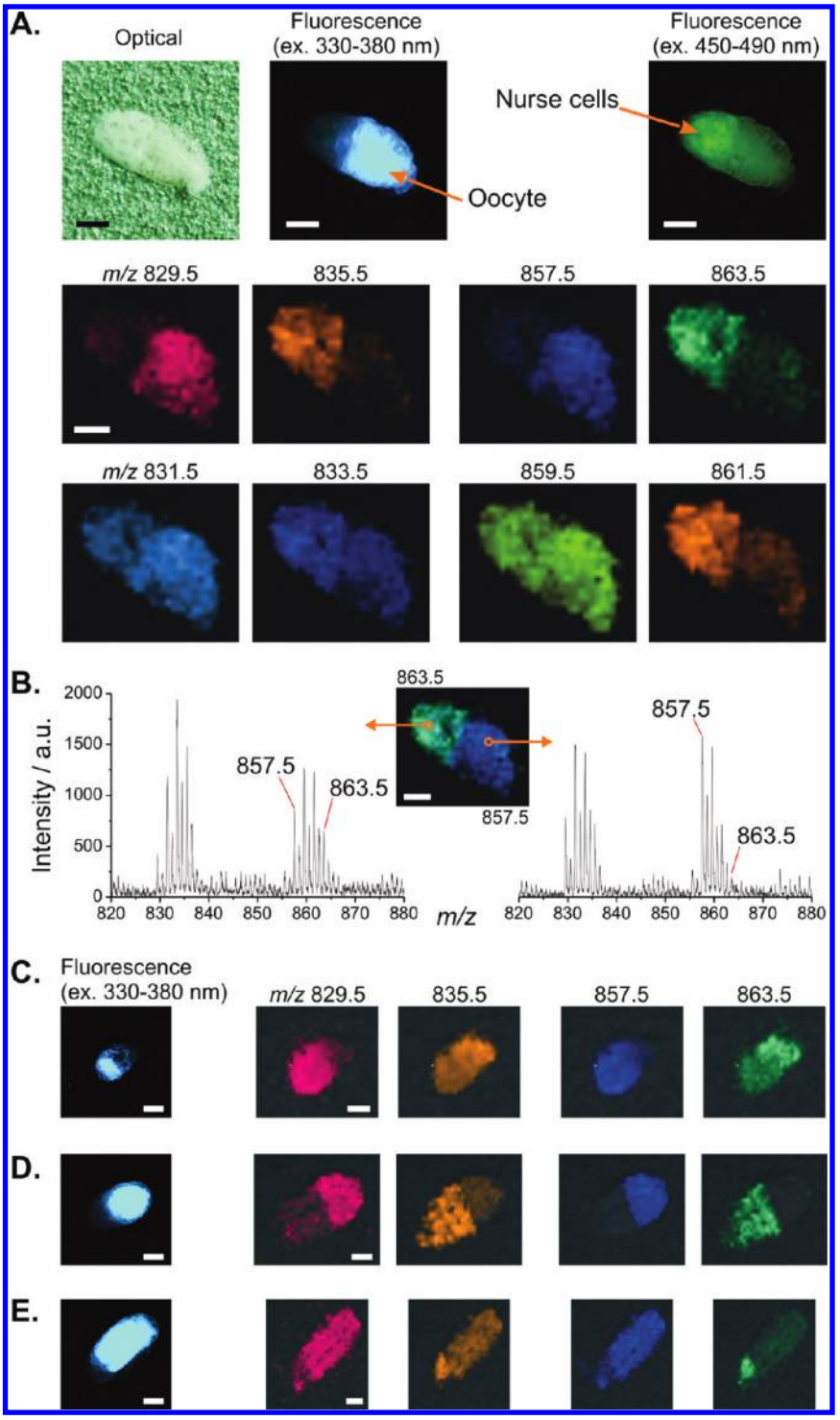

Figure 4. Optical, fluorescence, and MALDI images of individual egg chambers from fruit flies (*Drosophila melanogaster*) obtained according to the protocol presented. (A) An egg chamber in stage 10. (B) Mass spectra corresponding to the two points marked on the MALDI image of the specimen in A. (C−E) Egg chambers in different developmental stages (see the main text for details). (A−C) Strain w^{1118}, *p*{*ubi-nls-GFP*}; (D,E) strain w^{1118}. Labels in C also refer to D and E. Scale bars in A and C−E: 100 μm.

Following application of the 9-aminoacridine matrix, mass spectra were obtained (Figure 5C). Also in this case, the differences in the composition of polyunsaturated phosphatidylinositols in the oocyte and nurse-cell compartments are very clear. This proves that there are no major artifacts in the results obtained with the MS imaging protocol presented above.

Unsaturated acyl chains are essential for maintaining a certain level of membrane "fluidity".[20] Phosphatidylinositol is a significant membrane lipid, which also plays a role in cell signaling. In other work, differences in the distribution of phosphatidylinositols with various numbers of double bonds were observed in the tissue sections of the mouse embryo implantation site imaged by

dx.doi.org/10.1021/ac200481j |*Anal. Chem.* 2011, 83, 3918–3925

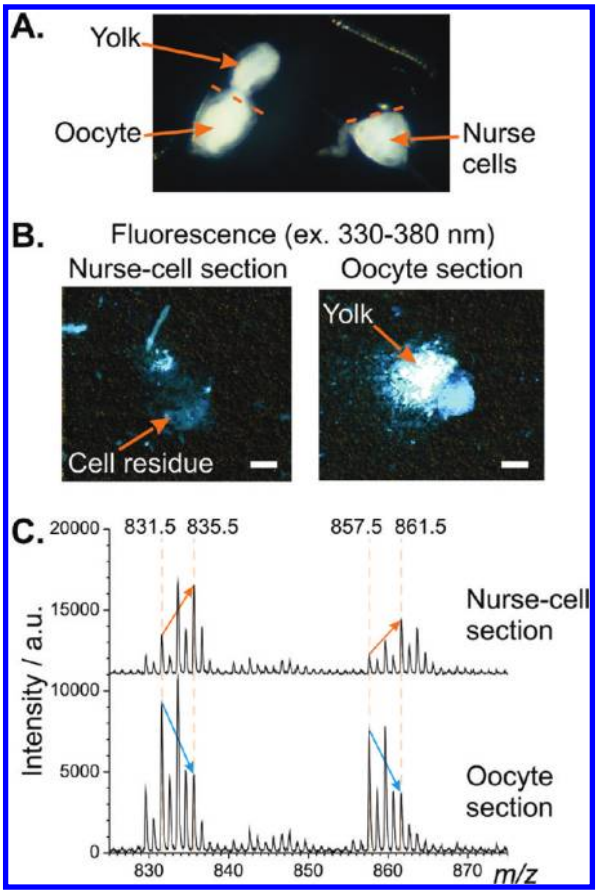

Figure 5. Verification of the gradient-like distribution of phospholipids within egg chambers. An egg chamber has been divided into the nurse-cell and oocyte sections. (A) Optical micrograph showing an egg chamber soon after a cut was made across the borderline between the nurse-cell and oocyte sections. Leakage of yolk from the oocyte is observed. Dashed lines indicate the cut sides. (B) Fluorescence micrographs showing the nurse-cell and oocyte sections deposited separately on the MALDI target. (C) MALDI spectra revealing distinct phospholipid patterns within the nurse-cell and oocyte compartments. Scale bar in B: 100 μm.

MALDI-MS.[50] While the relatively high abundance of phosphatidylinositols in the outer shell of egg chambers is biologically conceivable, we have gathered experimental evidence to prove that the phosphatidylinositols, detected in our experiments (Figure 4), are indeed present in the outer layers of egg chambers (that contain considerable amounts of lipid membranes): First, matrix crystals are not present inside the late-stage egg chambers prepared by the present protocol (Figure S2). By comparing micrographs of the matrix deposits on the egg chamber before and after MALDI imaging, it is easy to see that only a small portion of matrix was removed during the MS scan, while the sample has remained intact (Figure S6, Supporting Information). This is contrary to the previous study, in which algal cells were irradiated with a high-fluence laser beam and almost the entire contents of the cells were removed.[49] Second, in some samples of the late-stage egg chambers, primary metabolites such as adenosine triphosphate could mainly be detected within or around (after displacement) the oocyte part of the egg chamber, i.e., where follicle cells form a compact layer around the oocyte (Figure S7, Supporting Information): this supports the deduction that mainly the metabolically active easy-to-disrupt follicle layer around the oocyte is extracted with the matrix cocktail. Third, we analyzed sample preparation artifacts revealed by fluorescence microscopy. In some rare cases, the outer membranes of egg chambers were unintentionally ruptured, which resulted in the leakage or displacement of oocyte yolk within or outside the egg chamber (Figure S8, Supporting Information). Also in such cases, the segregation of phospholipids, as depicted in Figure 4, was maintained. Even damaging an egg chamber forcibly with a pipet tip did not blur the phospholipid gradient (Figure S9, Supporting Information). Fourth, the outer shell of the oocyte (cell membrane, follicle cells) was separated from yolk and deposited on a laser-ablated recipient site: high signals of phosphatidylinositols in the m/z ranges of 829.5−835.5 and 857.5−863.5 could still be recorded for this sample (Figure S10, Supporting Information). Despite this indirect evidence, one does not exclude a certain level of extraction and contribution of the phospholipid material contained inside the cells (follicle and nurse cells, as well as the oocyte) to the MS signals shown in Figures 3−5.

The results described above suggest that the phosphatidylinositols, whose gradient-like distribution is revealed in the MALDI images (Figure 4), are indeed present in the outer layer of egg chambers in the fruit fly. The high content of polyunsaturated phosphatidylinositols around the oocyte may be explained with the fact that the oocyte is rapidly expanding throughout oogenesis; therefore, high membrane fluidity is desirable to accommodate the increasing volume of this cell. One could also speculate that the observed gradient in the level of saturation of phosphatidylinositols along the anterior/posterior axis of egg chamber might be relevant for directing migration of border cells toward the oocyte.

CONCLUSIONS

The sample supports proposed here, which incorporate a rough recipient area, created by ablation with a microsecond-laser, help to immobilize biological specimens, absorb excess saline solution, accommodate microscopic observations, and facilitate application of a MALDI matrix onto the samples, avoiding major dispersion of phospholipid analytes. Ultrasound-assisted spray is seen to be a useful tool for application of MALDI matrixes to biological samples prior to imaging. The microscale MALDI imaging of intact egg chambers, according to the protocol presented above, reveals gradient-like distributions of several phospholipid species. These distributions closely match cell-level compartmentalization of egg chambers in several stages of oogenesis. The smallest distinguishable features are below 50 μm, which further emphasizes convergence of MALDI imaging with single-cell analysis. Because this micrometabolomic approach enables untargeted chemical mapping of the egg chamber assemblage, a follow-up study will implement this method in experiments on fruit flies with knock-downs of the genes that are involved in the regulation of cell migration in oogenesis. We believe that implementation of this protocol can gain further insight on the heterogeneity of lipid metabolism in the fruit fly. In the future, the protocol should also be extended toward vertical profiling of the lipid composition of egg chambers to enable differentiation between lipids in plasmalemma and intracellular membranes, in individual follicle cells, in nurse cells, and in the oocyte. Because small animals are used as model organisms in bioscience, the microscale imaging of lipid molecules

can thus provide important information for the understanding of developmental and signaling processes in general.

■ ASSOCIATED CONTENT

Supporting Information. Additional information as noted in the text. This material is available free of charge via the Internet at http://pubs.acs.org.

■ AUTHOR INFORMATION

Corresponding Author

*Tel: +886-3-5131527. Fax: +886-3-5723764. E-mail: yuchie@mail.nctu.edu.tw.

■ ACKNOWLEDGMENT

We acknowledge the fly core facility in Medical College, National Taiwan University, for providing the fruit fly strains, Dr. Yi-Sheng Wang (GRC, Academia Sinica) for allowing the use of the MALDI-FTICR-MS instrument, and Dr. Sabu Sahadevan and Mr. Alex Wang (Bruker Daltonics, Taiwan) for their support. We thank the National Science Council of Taiwan for the financial support of this work.

■ REFERENCES

(1) Edwards, J. L.; Kennedy, R. T. *Anal. Chem.* **2005**, *77*, 2201–2209.
(2) Sun, G.; Yang, K.; Zhao, Z.; Guan, S.; Han, X.; Gross, R. W. *Anal. Chem.* **2007**, *79*, 6629–6640.
(3) Amantonico, A.; Urban, P. L.; Fagerer, S. R.; Balabin, R. M.; Zenobi, R. *Anal. Chem.* **2010**, *82*, 7394–7400.
(4) Yukihira, D.; Miura, D.; Saito, K.; Takahashi, K.; Wariishi, H. *Anal. Chem.* **2010**, *82*, 4278–4282.
(5) Caprioli, R. M.; Farmer, T. B.; Gile, J. *Anal. Chem.* **1997**, *69*, 4751–4760.
(6) Cornett, D. S.; Reyzer, M. L.; Chaurand, P.; Caprioli, R. M. *Nat. Methods* **2007**, *4*, 828–833.
(7) Reyzer, M. L.; Caprioli, R. M. *Curr. Opin. Chem. Biol.* **2007**, *11*, 29–35.
(8) Fournier, I.; Wisztorski, M.; Salzet, M. *Expert Rev. Proteomics* **2008**, *5*, 413–424.
(9) Walch, A.; Rauser, S.; Deininger, S. O.; Höfler, H. *Histochem. Cell Biol.* **2008**, *130*, 421–434.
(10) Chughtai, K.; Heeren, R. M. A. *Chem. Rev.* **2010**, *110*, 3237–3277.
(11) Svatoš, A. *Trends Biotechnol.* **2010**, *28*, 425–434.
(12) Chaurand, P.; Cornett, D. S.; Angel, P. M.; Caprioli, R. M. *Mol. Cell. Proteomics* **2011**, *10*, 1–11.
(13) Römpp, A.; Guenther, S.; Schober, Y.; Schulz, O.; Takats, Z.; Kummer, W.; Spengler, B. *Angew. Chem., Int. Ed.* **2010**, *49*, 3834–3838.
(14) Roberts, D. B. *Drosophila: A Practical Approach*; Oxford University Press, Oxford, 1998.
(15) Dahmann, C., Ed. *Drosophila: Methods and Protocols*; Humana Press: Totowa, NJ 2010.
(16) Montell, D. J. *Nat. Rev. Mol. Cell Biol.* **2003**, *4*, 13–24.
(17) Renault, A. D.; Sigal, Y. J.; Morris, A. J.; Lehmann, R. *Science* **2004**, *305*, 1963–1966.
(18) Schultz, C. *Nat. Chem. Biol.* **2010**, *6*, 473–475.
(19) Feller, S. E.; Gawrisch, K.; MacKerell, A. D., Jr. *J. Am. Chem. Soc.* **2002**, *124*, 318–326.
(20) Hulbert, A. J. *J. Exp. Biol.* **2003**, *206*, 2303–2311.
(21) Puolitaival, S. M.; Burnum, K. E.; Cornett, D. S.; Caprioli, R. M. *J. Am. Soc. Mass Spectrom.* **2008**, *19*, 882–886.
(22) Ridenour, W. B.; Kliman, M.; McLean, J. A.; Caprioli, R. M. *Anal. Chem.* **2010**, *82*, 1881–1889.
(23) Vidová, V.; Pól, J.; Volný, M.; Novák, P.; Havlíček, V.; Wiedmer, S. K.; Holopainen, J. M. *J. Lipid Res.* **2010**, *51*, 2295–2302.
(24) Taira, S.; Sugiura, Y.; Moritake, S.; Shimma, S.; Ichiyanagi, Y.; Setou, M. *Anal. Chem.* **2008**, *80*, 4761–4766.
(25) Vidová, V.; Novák, P.; Strohalm, M.; Pól, J.; Havlíček, V.; Volný, M. *Anal. Chem.* **2010**, *82*, 4994–4997.
(26) Rubakhin, S. S.; Greenough, W. T.; Sweedler, J. V. *Anal. Chem.* **2003**, *75*, 5374–5380.
(27) Hölscher, D.; Shroff, R.; Knop, K.; Gottschaldt, M.; Crecelius, A.; Schneider, B.; Heckel, D. G.; Schubert, U. S.; Svatoš, A. *Plant J.* **2009**, *60*, 907–918.
(28) Monroe, E. B.; Jurchen, J. C.; Lee, J.; Rubakhin, S. S.; Sweedler, J. V. *J. Am. Chem. Soc.* **2005**, *127*, 12152–12153.
(29) Fletcher, J. S.; Rabbani, S.; Henderson, A.; Blenkinsopp, P.; Thompson, S. P.; Lockyer, N. P.; Vickerman, J. C. *Anal. Chem.* **2008**, *80*, 9058–9064.
(30) Szakal, C.; Narayan, K.; Fu, J.; Lefman, J.; Subramaniam, S. *Anal. Chem.* **2011**, *83*, 1207–1213.
(31) Romanova, E. V.; Rubakhin, S. S.; Monroe, E. B.; Sweedler, J. V. In *Single Cell Analysis: Technologies and Applications*; Anselmetti, D., Ed.; Wiley-VCH Verlag: Weinheim, 2009.
(32) Kruse, R.; Sweedler, J. V. *J. Am. Soc. Mass Spectrom.* **2003**, *14*, 752–759.
(33) Zimmerman, T. A.; Rubakhin, S. S.; Romanova, E. V.; Tucker, K. R.; Sweedler, J. V. *Anal. Chem.* **2009**, *81*, 9402–9409.
(34) Cornett, D. S.; Frappier, S. L.; Caprioli, R. M. *Anal. Chem.* **2008**, *80*, 5648–5653.
(35) Aerni, H. R.; Cornett, D. S.; Caprioli, R. M. *Anal. Chem.* **2009**, *81*, 7490–7495.
(36) Benabdellah, F.; Touboul, D.; Brunelle, A.; Laprévote, O. *Anal. Chem.* **2009**, *81*, 5557–5560.
(37) Mangé, A.; Chaurand, P.; Perrochia, H.; Roger, P.; Caprioli, R. M.; Solassol, J. *J. Proteome Res.* **2009**, *8*, 5619–5628.
(38) Prasad, M.; Jang, A. C. C.; Starz-Gaiano, M.; Melani, M.; Montell, D. J. *Nat. Protoc.* **2007**, *2*, 2467–2473.
(39) Urban, P. L.; Amantonico, A.; Zenobi, R. *Mass Spectrom. Rev.* **2011**, *30*, 435–478.
(40) McLauchlin, M. L.; Yang, D.; Aella, P.; Garcia, A. A.; Picraux, S. T.; Hayes, M. A. *Langmuir* **2007**, *23*, 4871–4877.
(41) Torta, F.; Fusi, M.; Casari, C. S.; Bottani, C. E.; Bachi, A. *J. Proteome Res.* **2009**, *8*, 1932–1942.
(42) Amantonico, A.; Flamigni, L.; Glaus, R.; Koch, J.; Günther, D.; Zenobi, R. Nanostructured Surfaces Produced by Laser Ablation as Substrates for Metabolome Analysis via Laser Desorption/Ionization Mass Spectrometry. Presented at the ASMS Conference, Denver, CO, May 31—June 4, 2009.
(43) Urban, P. L.; Jefimovs, K.; Amantonico, A.; Fagerer, S. R.; Schmid, T.; Mädler, S.; Puigmarti-Luis, J.; Goedecke, N.; Zenobi, R. *Lab Chip* **2010**, *10*, 3206–3209.
(44) Vermillion-Salsbury, R. L.; Hercules, D. M. *Rapid Commun. Mass Spectrom.* **2002**, *16*, 1575–1581.
(45) Miura, D.; Fujimura, Y.; Yamato, M.; Hyodo, F.; Utsumi, H.; Tachibana, H.; Wariishi, H. *Anal. Chem.* **2010**, *82*, 9789–9796.
(46) Jung, H. Y.; Park, H. J.; Calo, J. M.; Diebold, G. J. *Anal. Chem.* **2010**, *82*, 10090–10094.
(47) Jurchen, J. C.; Rubakhin, S. S.; Sweedler, J. V. *J. Am. Soc. Mass Spectrom.* **2005**, *16*, 1654–1659.
(48) Vrkoslav, V.; Muck, A.; Cvačka, J.; Svatoš, A. *J. Am. Soc. Mass Spectrom.* **2010**, *21*, 220–231.
(49) Urban, P. L.; Schmid, T.; Amantonico, A.; Zenobi, R. *Anal. Chem.* **2011**, *83*, 1843–1849.
(50) Burnum, K. E.; Cornett, D. S.; Puolitaival, S. M.; Milne, S. B.; Myers, D. S.; Tranguch, S.; Brown, H. A.; Dey, S. K.; Caprioli, R. M. *J. Lipid Res.* **2009**, *50*, 2290–2298.